Investigations Properties on the Corrosion Inhibition of *Kala Bansa* Leaf Extract on Mild Steel in an Acidic Environment

O. S. Yadav[1], S. Kumar[1], K. Yadav[1], R. Sharma[1] and R. Kumar[2]

[1]*Shyamlal College Department of Chemistry Shahdara, Delhi, India*
[2]*Shyamlal College Department of Physics Shahdara, Delhi, India*
Corresponding author: opduchem@gmail.com

Received 20/12/2023; accepted 26/04/2024
https://doi.org/10.4152/pea.2026440103

Abstract
Different Ct of KBE from its leaves were used to study its effect on MS corrosion resistance. Electrochemical methods such as PDP, EIS and WL tests were herein used. Experimental results showed that, with higher Ct of KB, its IE(%) increased. The highest corrosion IE(%) of 98.41, at 1600 ppm KBE in a 0.5 M H_2SO_4 solution, was obtained. The inhibitor's adsorption onto the MS surface was excellent, since it created a monolayer. KBE´s adsorption mechanism obeyed Langmuir's isotherm. SEM analysis established the development of a protective layer on the MS surface.

Keywords: CI; EIS; LPR; PDP;SEM; WL.

Introduction•

For a long time, steels and its alloys have been used in several industries for various purposes, such as pipelines. Every year, worldwide economic losses caused by corrosion amount to 75,000 billion dollars, which depletes world's GDP of 3-4% [1]. Metals corroding process may be prevented with the aid of CI [2, 3], which hinder metals dissolution by mineral acids attacks. Several types of un-eco friendly and toxic CI are used in industries, some of which are inorganic and organic synthesized substances. Nowadays, green and nontoxic CI are in high demand.
Various industries employ acids in the process of cleaning pipes and oil from surfaces [4-6]. CI usually behaves as adsorbents, which means they adsorb onto metals surfaces and form a chemical bond. However, there are some phenomena where they are attracted by metals, originating physical adsorption. Different plant parts are used to prepare green CI extracts, since they have good ability to cover metals surfaces, because their photochemical components possess aromatic structures with hetero atoms. Generally, CI added to AE has organic molecules that contain hetero atoms as prime chemical constituents. In several studies, the extracts of many plants have been used as efficient CI in various AE, such as: walnut green (*Juglans regia L.*) husk [7];

•The abbreviations and symbols definition lists are in pages 39-40.

Mish Gush [8], *Stachys byzantine* [9], *Thymus vulgaris* [10] and *Aloysia citrodora* [11] leaves; *Punica granatum* peel on SS-410 [12]; *Ammi visnaga* (which was also used as friendly antioxidant) [13]; *Allamanda cathartica* [14], and *Senggani* (*Melastoma candidum D. don*) [15] leaves; and iodide ions and *Xanthium strumarium* leaves [16].

KB is a deciduous flowering plant with diverse genera, of the *Acanthaceae* family. It is an Indian routine medicinal plant, which is used in various treatments of ailments. Its leaves contain various type of photochemical [17, 18], such as saponins, flavonoids and glycosides.

The novelty of the present work was to employ KBE as a green CI for MS in H_2SO_4. Employed electrochemical techniques were EIS, PDP and LPR, to test whether KBE behaved as a mixed-type CI. KB adsorption onto the MS surface in H_2SO_4 followed Langmuir's isotherm.

Materials and methods

KBE preparation

KBE was obtained via maceration process from 80% ethanol/water system. Then, it was filtered. The residues were removed by a solvent and eliminated via rotary evaporator. A concentrated blackish solid was obtained.

WL method

WL is an extensively used and predictable method for estimating CR. The prepared blank solution was made of geared 0.5 M H_2SO_4 (analytical reagent) and distilled water. CR values of MS were evaluated at different T (298, 308, 318 and 328 K), via WL method, with different Ct of KBE in the test solution, for 20 h. MS samples (1 x 1 x 1 cm) had the chemical composition by wt% of C-0.1, Si-0.033, Mn-0.335, Al-0.057, Cu-0.0476, Cr-0.02 and balance Fe. For 20 h, the MS samples were entirely immersed in a conical flask of 250 cm^3 with a 0.5 M H_2SO_4 solution. Then, they were taken from the test solutions, and cleaned with acetone.

Instrumentation (electrochemical) measurements

Selected Ct ranges of KBE solutions for the current study were 400, 800, 1200 and 1600 ppm. They were diluted in 0.5 M H_2SO_4, which was also used as blank. All steps of this experimentation and measurement employed scientific programs have been delineated elsewhere [19-22]. The electrochemical potentiostat study was performed by CH Instruments, Inc.CHI760c. The SR adopted in PDP study was 1.0 mV/s^{-1}. EIS were recorded with an amplitude of 5 mV peak to peak, at OCP, with signals/disturbance in the frequency range from 10^5 to 10^{-2} Hz.

Study of surface characterization

MS coupons (1 × 1 cm × 2 mm) were used for the surface characterization study. Polished MS coupons were subjected to corrosion, in H_2SO_4, at the Ct range of KBE from 400 to 1600 ppm, to monitor IE(%), for 10 h. SEM studies were performed by Jeol Japan, Model No. JSM-6610 LV instrument.

GC-MS study

GC-MS study was performed with a Shimadzu GC–MS-QP 2010 Ultra fitted with an RTX-5 MS (30 m x 0.25 mm x 0.25 µm) capillary column. He gas was used as transporter, with the flow rate of 1.21 mL /min. The initial oven T was 60 ºC, for two min, and then it was increased to 260 ºC. The 2 mL sample was injected in split less mode, and total IT was 60 min. The ions source was heated at 220 ºC, and electron-impact ionization technique was used at a potential of 70 eV. Mass spectra of KBE with crude ethanol showed compounds identified from NIST and WILEY libraries, and their assessment agreed with those reported in literature [23].

Results and discussion

WL calculation

Data calculated via WL are listed in Table 1.

Table 1: WL parameters for MS, for 20 h IT in 0.5 M H_2SO_4 without and with KBE at various Ct and T (298-328 K).

T	Ct (ppm)	WL (mg)	CR ($mg/cm^{-2}/h^{-1}$)	IE%	SC (θ)
298 K	Blank	0.4979	0.0277	-	-
	400	0.0471	0.0026	90.61	0.9061
	800	0.0362	0.0016	94.22	0.9422
	1200	0.0202	0.0011	96.02	0.9602
	1600	0.0092	0.0005	98.19	0.9819
308 K	Blank	0.6187	0.0345	-	-
	400	0.0599	0.0034	90.14	0.9014
	800	0.0395	0.0022	93.62	0.9362
	1200	0.0260	0.0014	95.94	0.9594
	1600	0.0175	0.0009	97.39	0.9739
318 K	Blank	0.8261	0.0460	-	-
	400	0.0872	0.0048	89.56	0.8956
	800	0.0710	0.0039	91.52	0.9152
	1200	0.0598	0.0033	92.82	0.9282
	1600	0.0361	0.0020	95.65	0.9565
328 K	Blank	1.0471	0.0584	-	-
	400	0.2725	0.0152	73.97	0.7397
	800	0.1681	0.0093	84.07	0.8407
	1200	0.1051	0.0058	90.06	0.9006
	1600	0.0705	0.0039	93.32	0.9332

Due to MS corrosion in a 0.5 M H_2SO_4 solution, its WL was examined, with various Ct of KBE, at several T (298, 308, 318 and 328 K). CR (mm/yr^{-1}) was calculated using eq. (1).

$$C_R = \frac{KxW}{Axtx\rho} \quad (1)$$

where W is WL, t is IT, ρ is density (7.85 g/cm^3) and K denotes corrosion constant (8.76×10^4) [24]. C_R^A and C_R^i are CR of MS in H_2SO_4 without and with KBE, of which effect on CR is shown in Fig. 1.

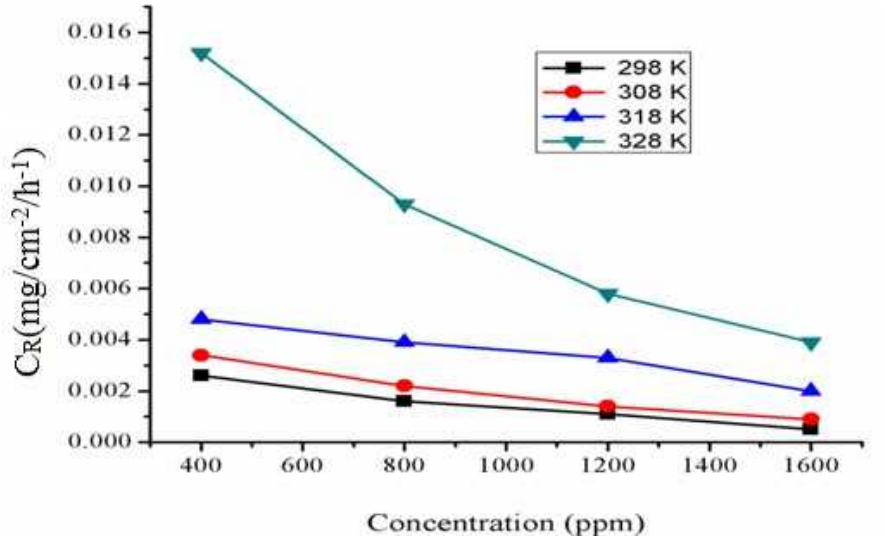

Figure 1: CR values with different Ct of KBE at T from 298 to 318 K.

With higher Ct of KBE, CR decreased, as shown in Fig. 2. The inhibitor's molecules were adsorbed onto the MS surface, which hindered CR. The lower the Ct from KBE, the lower the IE(%).

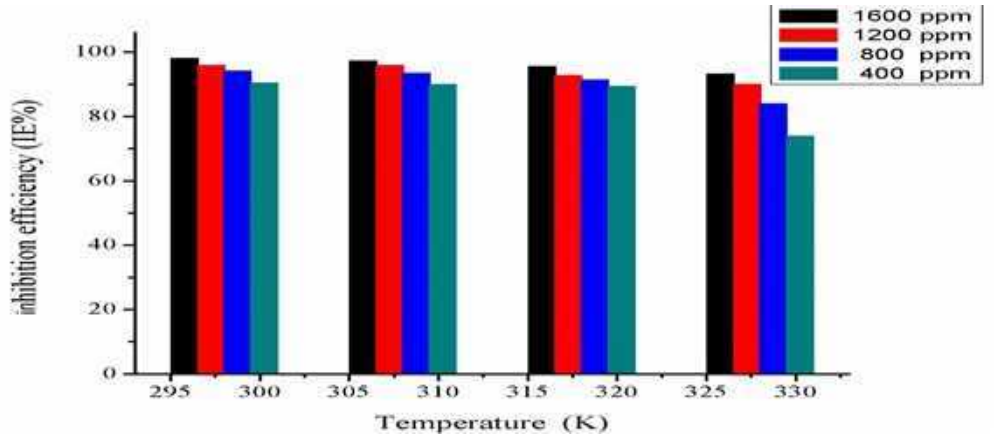

Figure 2: Variation in IE(%)with various Ct of KBE, at T from 298 to 328 K.

From Table 1, maximum IE(%) of KBE was 98.19, which was achieved at a Ct of 1600 ppm. The inhibitor's IE(%) and SC (θ) values were calculated via eqs. (2) and (3), respectively.

$$IE(\%) = \frac{C_R^A - C_R^i}{C_R^A} X\ 100 \quad (2)$$

$$SC(\theta) = \frac{C_R^A - C_R^i}{C_R^A} \quad (3)$$

Polarization investigations

Galvanostatic study and LRP

Polarization analyses were carried out thorough determination of KBE inhibition mechanism, at 298 K, using different Ct. From the experimental study, Tafel curve plot is shown in Fig. 3, and polarization is represented by Table 2. Improvement in corrosion IE(%) via i_{corr} was calculated by Eq. (4).

$$Tafel(IE\%) = \frac{I_{acid} - I_{inh}}{I_{acid}} X \ 100 \qquad (4)$$

where I_{inh} and I_{acid} are I_{inh} values without and with KBE in a 0.5 M H_2SO_4 solution, respectively.

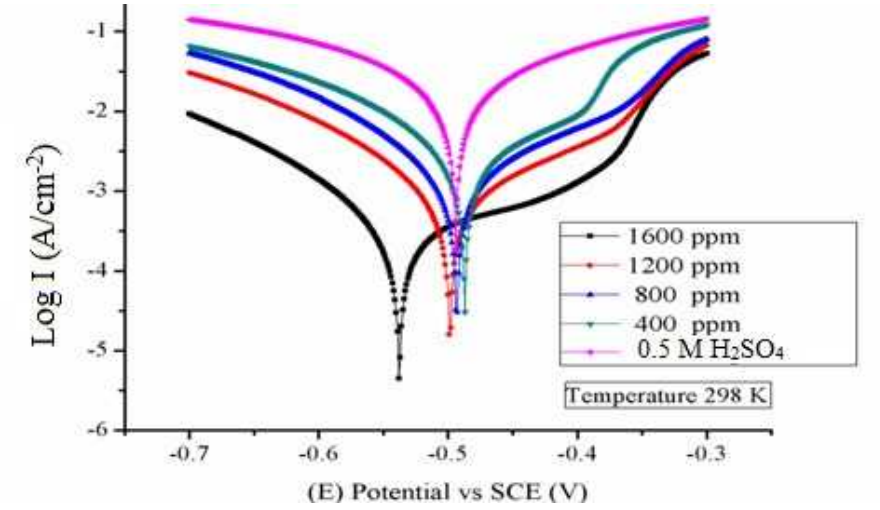

Figure 3: Galvanostatic polarization curves for MS in a 0.5 M H_2SO_4 solution with various Ct of KBE, at 298 K.

Table 2: Tafel and LPR parameters for MS in a 0.5 M H_2SO_4 solution with different Ct of KBE, at 298 K.

Ct (ppm)	I_{corr} (A/cm^2)	E_{corr} (mV per SCE)	IE%	Tafel data		LPR data	
				βc (mV/dec)	βa (mV/dec)	R_p (Ω/cm^2)	LPR%
Blank	2.560	0.494	-	53.81	51.47	1.6	-
400	0.2165	0.487	91.54	73.45	98.54	15.4	89.57
800	0.1803	0.493	92.95	67.30	86.80	18.7	91.44
1200	0.09865	0.499	96.14	70.52	85.25	31.3	94.88
1600	0.04067	0.538	98.41	91.01	45.38	78.4	97.95

CI action in 0.5 M H_2SO_4 improved with higher Ct of KBE. E_{corr} experimental values' trend means that the inhibitor is an anti-corrosion catalyst of mixed type. With KBE, β_a and β_c noticeably changed in an irregular manner, due to the inhibition process that implied HER and MS dissolution. β_a was mainly slower than

β_c, phenomenon that may be temporary, as indicated by the suppressed anodic reaction of MS oxidation/dissolution via KBE action. Moreover, β_c differed, although slightly, and the inhibitor suppressed HER. Both reactions were limited by KBE-Fe complexes ($[Fe\text{-}atoms\text{-}KBE]_{ads}$) and [Fe- atoms- KBE -OH]$_{ads}$) on the substrate's surface, which led to complete active sites coverage [25]. LPR values specify KBE's adsorption onto the MS surface by the development of a physical barrier with a non-conducting nature.

EIS measurements

EIS experiments were performed to assess inter facial changes at the MS surface in 0.5 M H_2SO_4 with and without KBE, at 298 K. This study was used as a separate and additional method to properly measure IE(%), mechanistic and kinetic data of the electrochemical system under examination. Resulting Bode and Nyquist plots are shown in Figs. 4 and 5, and their parameters are specified in Table 3.

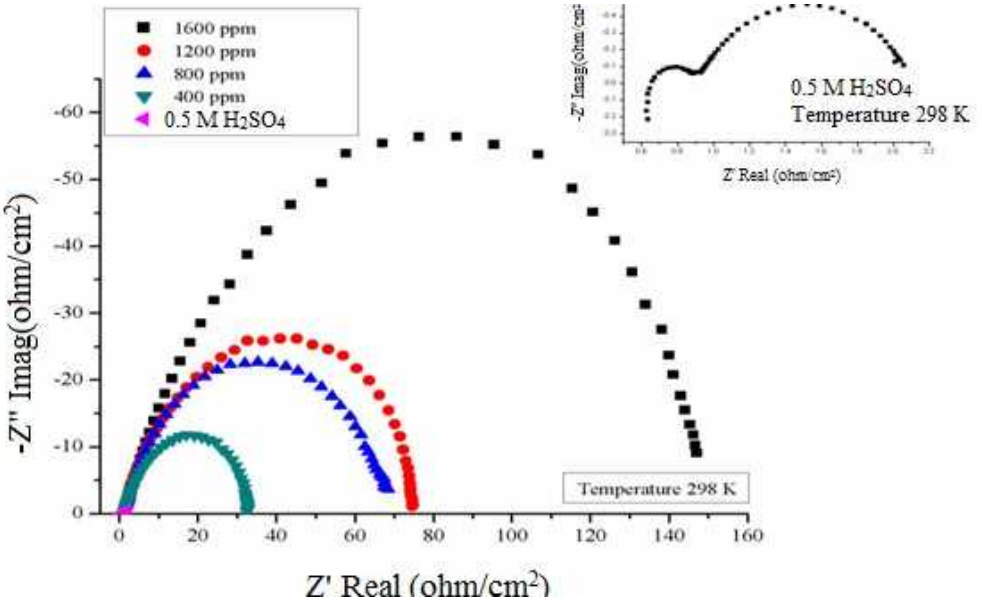

Figure 4: Nyquist's plots for MS in a 0.5 M H_2SO_4 solution without and with KBE at various Ct, at 298 K.

The MS's surface irregularity and CI mechanism via single charge transfer was considered through the single semi-circle in the Nyquist plot, for all Ct of KBE in H_2SO_4 [26]. The diameter in R_{ct} remarkable rose with increased Ct of the inhibitor, which confirmed this mechanism. CR of MS decreased, after KBE created an insoluble protective layer. By using Eq. (5), IE(%) values were calculated [27].

$$(EIS)IE(\%) = \frac{R_{Ct} - R^{a}_{Ct}}{R_{Ct}} \times 100 \qquad (5)$$

where R_{ct} and R^{a}_{Ct} are R_{ct} values with and without KBE, respectively.

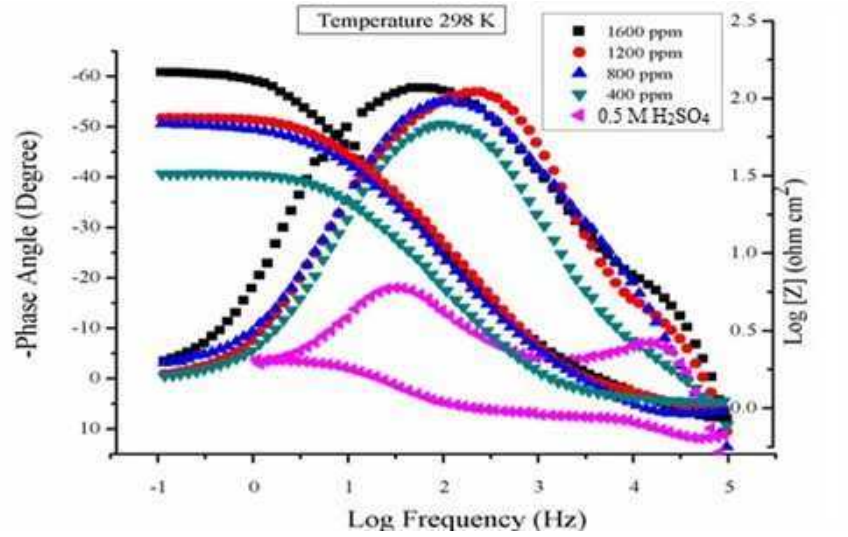

Figure 5: Bode's plot for MS in a 0.5 M H_2SO_4 solution without and with KBE in various Ct, at 298 K.

Table 3: Parameters of impedance for MS in 0.5 M H_2SO_4 without and with KBE, in various Ct, at 298 K.

Ct (ppm)	R_s (Ω/cm^2)	n	Q ($\Omega^{-1}/cm^{-2}\ S^n$)	R_{ct} (Ω/cm^2)	F_{max} (Hz)	C_{dl} (F/cm^{-2})	IE%
Blank	1.4	0.7105	0.876	1.720	6.50	0.14229	
400	1.2	08528	0.481	30.19	14.31	0.03682	94.38
800	1.3	08974	0.116	70.31	17.28	0.001312	97.55
1200	1.4	0.9296	0.0424	75.37	23.39	0.0007996	97.71
1600	1.1	0.9510	0.016	155.77	69.75	0.0001464	98.89

C_{dl} was measured by using Eq. (6), of which values increased with higher Ct of KBE.

$$Cdl = \frac{1}{2\pi R_{Ct} f_{max}} \quad (6)$$

where f_{max} is maxima frequency via Nyquist curve.
Eq. (7) represents an inverse relation between C_{dl} and thickness (d) of the shielding layer. Experimental parameters are listed in Table 3, which shows a decrease in C_{dl} value with higher Ct of KBE. This means that the protecting layer thickness increased.

$$Cdl = \frac{A\varepsilon\varepsilon_0}{d} \quad (7)$$

where A is the surface area of the MS substrate, Ɛ and Ɛo are constants dielectric for the vacuum permittivity with the medium and d is the shielding layer thickness.
The significance of single time constant is illustrated by Bode graphs of Fig. 5, for each Ct of KBE. The phase angle approached to 90^0, which was further confirmed by stronger homogeneous MS surface substrate [28]. Other parameters include (n)

values phase shift from Eq. (8), which are nearer to unity with KBE addition, and associated with less heterogeneity on the MS surface without inhibitor [29-31].

$$Cdl = Q(\omega)^{n-1} = Q(2\pi f_{Zim-max})^{n-1} \quad (8)$$

where Q is CPE, ω is angular frequency, which is an imaginary part with the maximum value of electrochemical impedance plot and $f_{Zim-max}$ is maxima frequencies.

Study of T's kinetics

Adsorption isotherm

The relation between KBE's molecules and the MS's surface was studied via the adsorption mechanism characteristics, employing various isotherms. Experimental data established that the relation with best fit was for Langmuir's adsorption isotherm, with linearR^2values (0.999 - 1) obtained by the plotting graph C/θ *vs*. Ct, at different T, which generated straight lines [32-37] (Fig. 6).

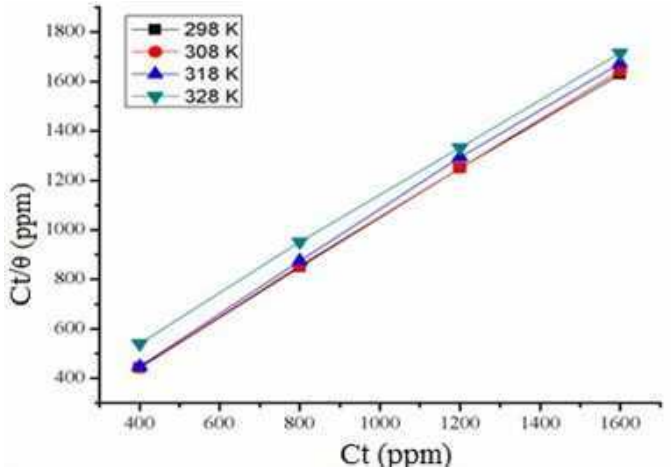

Figure 6: Langmuir's isotherm for KBE (at different Ct) adsorption onto MS in a 0.5 M H_2SO_4 solution, at various T.

From Eq. (9), Langmuir's isotherm was calculated. It depends on the Ct of KBE's molecules in the H_2SO_4 solution, which have performed SC (θ) of MS.

$$\frac{C_{inh}}{\theta} = \frac{1}{K_{ads}} + C_{inh} \quad (9)$$

where C_{inh} is Ct of KBE (Fig. 7). R^2 value had a recognized major role on the relations between KBE's molecules adsorbed on to the MS surface substrate, which were linked on to cathodic and anodic reactive sites. In the investigated system, the additive molecules blankets on cathodic and anodic sites were formed by the adsorption mechanism and the development of a multi-molecular layer that obeyed Langmuir's isotherm.

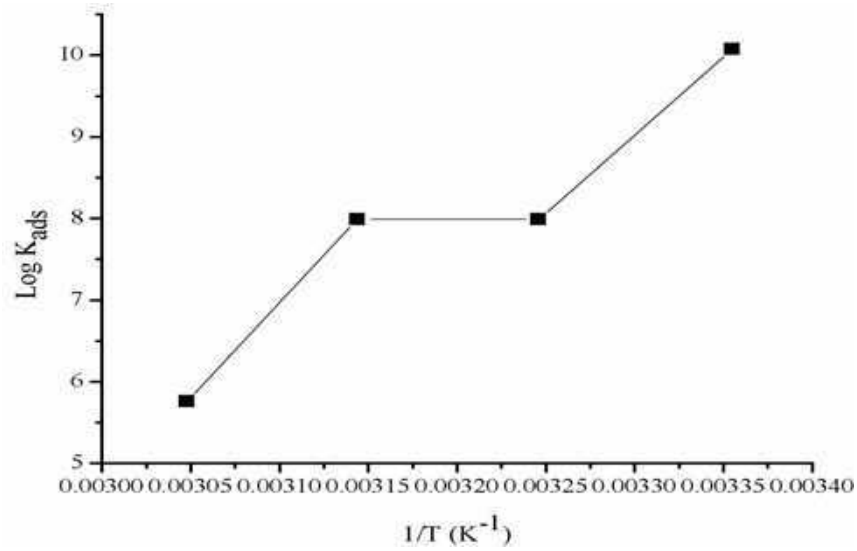

Figure 7: Graph (logK_{ads} versus 1/T) of$\Delta G°_{ads}$KBE on the MSsurface.

K_{ads} values were employed to determine $\Delta G°_{ads}$ via Eq. (10), indicating KBE strong adsorption onto the MS surface. The adsorption was strong, since more hetero atoms with lone pair and aromatic rings were delocalized from pi electrons in KBE's molecules. According to [38], $\Delta G°_{ads}$ values closer to -40 kJ/mol^{-1} indicate chemisorption, and those nearer to -20 kJ/mol^{-1} show physisorption. For this study, calculated values and parameters are listed in Table 4, which were near to -40 kJ/mol^{-1}, at different T, revealing a chemisorption process, which indicates its spontaneous nature.

Table 4: Thermodynamic parameters for KBE's adsorption onto the MS surface in 0.5 M H_2SO_4, at different T.

T	Log K	R^2	ΔH_{ads} (kJ/mol)	ΔS_{ads} (j/mol/K)	ΔG_{ads} (kJ/mol)
298	6.29	0.9997	-51.65	-49.22	-45.83
308	5.31	0.9999			-41.59
318	5.30	0.9993			-42.88
328	4.79	0.9997			-41.02

$$\Delta G^{o}_{ads} = -2.303RT\,[\log(55.5) + \log K_{ads}] \quad (10)$$

where R is universal gas constant. The water's molecule Ct was 55.5 mol/L.
In the present study, obtained $\Delta S°_{ads}$ value was -49.22 kJ/mol, which suggested that the arrangement of KBE's molecules on the MS surface followed the process of exothermic adsorption [39].

E_a parameter and T effect

The study of T effect, via WL calculations, on MS (coupon) in 0.5 M $H_2SO_4$with different Ct of KBE, is listed in Table 1, which shows CR, SC (θ) and IE(%)values.

In the solution without KBE, CR of MS exponentially rose from 298 to 328 K, whereas with the inhibitor, it slightly decreased. IE(%) declined with T rise from 298 to 328 K. By using Arrhenius equation (11), E_a was determined [40].

$$\log \partial = \log A - \frac{E_a}{2.303\ RT} \quad (11)$$

where A is pre-exponential factor of Arrhenius. The plot derived by Arrhenius and Eyring equations is shown in Fig. 8.

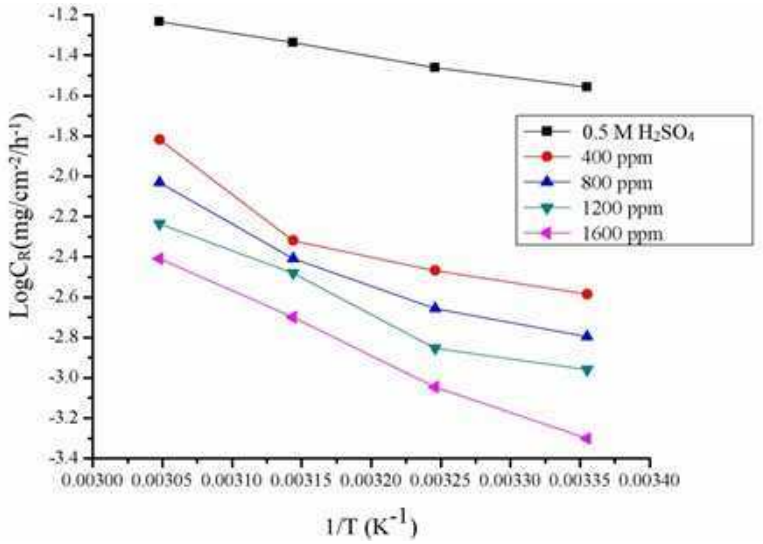

Figure 8: Arrhenius plots of Log CR against T^{-1} for MS in a 0.5 M H_2SO_4 solution containing different Ct of KBE.

Calculated values for $\Delta H°_{ads}$ and $\Delta S°_{ads}$ are listed in Table 5. E_a values were calculated via a straight line of the slope (E_a = slope x 2.303 R^2), resulting from Arrhenius plot log ∂ *vs.* 1/T curve. E_a observed value for the systems with KBE were larger than those without it, which suggests that the adsorption process was chemical. $\Delta H°_{ads}$ and $\Delta S°_{ads}$ values were calculated by using Eq. (12).

$$\partial = \frac{RT}{Nh} \exp\left(\frac{\Delta S^o_{ads}}{R}\right) \exp\left(-\frac{\Delta H^o_{ads}}{RT}\right) \quad (12)$$

where N is Avogadro number and h is Plank constant [41].

Table 5: E_a parameters for MS in 0.5 M H_2SO_4 with and without KBE in different Ct.

Ct (ppm)	E_a (kJ/mol)	ΔH^o_{ads} (kJ/mol)	ΔS^o_{ads} (j/mol/K)
1600	56.49	54.24	-110.21
1200	47.30	44.98	-74.11
800	47.25	44.25	-73.98
400	45.37	42.81	-61.29
Blank	20.44	19.11	-120.87

Through the adsorption route, reactants molecules were improved to activate the complex, in which the phyto chemicals disordering took place. $\Delta S°_{ads}$ negative values reveal the associative mechanism that marks the progress of an activated complex, of which step was rate determining [42]. $\Delta S°_{ads}$ positive values correspond to the endothermicity of MS's dissolution reaction. They were higher with KBE, which means that the energy barrier for MS dissolution reaction was drastically improved by the CI in H_2SO_4 [23].

Morphological investigation

SEM

The micrographs (Figs. 9a-9d) obtained via SEM in a 0.5 M H_2SO_4 solution with out and with KBE (1600 and 400 ppm) show the changes caused by the corrosion process.

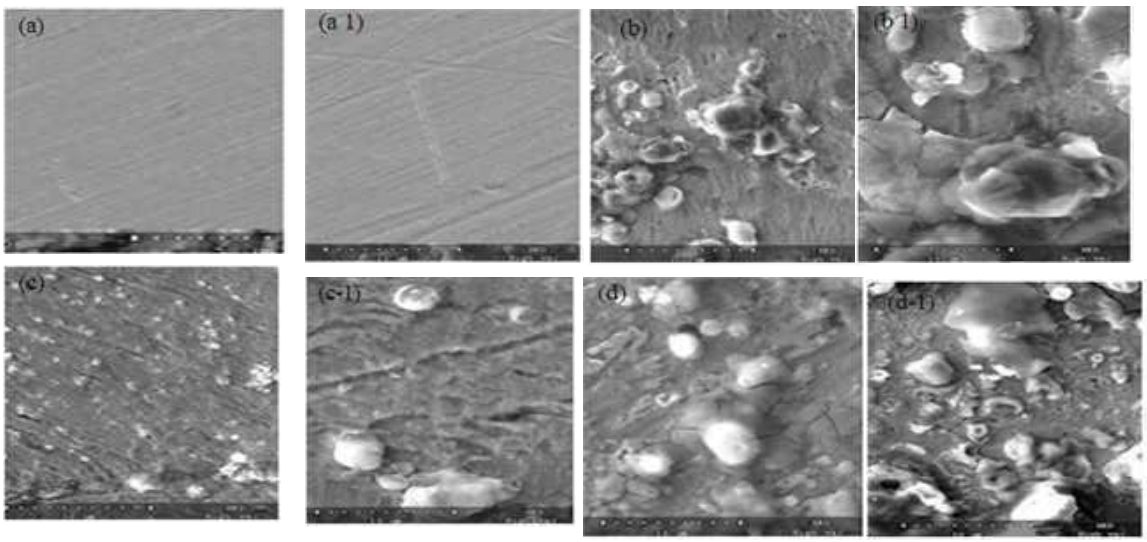

Figure 9: SEM micrographs with magnification 1000 (1) 3000 of MS surfaces - **(a)** bare; with 0.5 M H_2SO_4-**(b)** blank, **(c)**with 1600 ppm KBE, and (**d)** with 1200 ppm KBE.

The MS surface in 0.5 M H_2SO_4 was damaged, as shown in Fig 9 (b). Its morphology appreciably improved (Fig. 9c) with the addition of 1600 ppm KBE, and less damages occurred compared to the sample with blank 0.5 M H_2SO_4. The MS surface roughness level was reduced when the Ct of KBE was increased from 400 to 1600 ppm. This enhancement in MS morphology was due to the excellent protective layer [43, 44] formed by KBE on its surface, which was responsible for CI.

GC-MS analysis

In the current investigation, GC-MS identified 15 compounds among the 45 constituents recognized in MS immersed in KBE with ethanol, as shown in Fig.10.

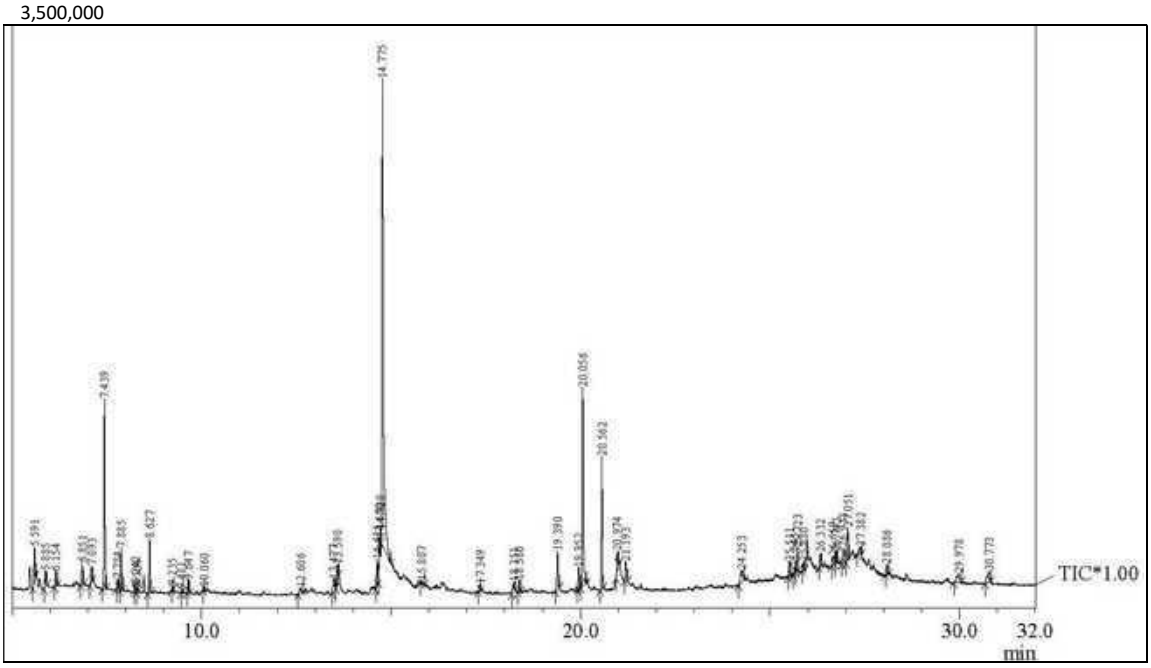

Figure 10: GC-MS of MS and KBE.

Table 6 characterizes the identified compounds, such as their MF, MW, IT, PA and SI. The phytochemical examination of KBE exposed the presence of heterocyclic organic compounds that can be largely classified as sterols, long chain alkenes (cyclic), long chain fatty acids and purine nucleosides. The majority of detected phytocomponents have been reported as effective green CI [45-52]. The existence of multiple bonds with electrons, hetero atoms and some other substances in these organic compounds provides for excellent CI properties [53], due to the synergy among all of them.

Table 6: Phytocomponents detected in KBE.

S. no	Compounds	MF	MW	IT	PA%	SI
1	1,2,4-trimethylbenzene	C_9H_{12}	120	5.885	0.98	93
2	Cyclopropylbenzene	C_9H_{10}	118	6.851	1.28	93
3	3a,4,5,6,7,7a-hexahydro-4,7-methanoindene	$C_{10}H_{14}$	134	7.439	9.22	96
4	4,7-Methano-1H-indene, octahydro-	$C_{10}H_{16}$	136	7.885	2.03	95
5	Tricyclo[5.2.1.0(2,6)]dec-4-ene, 4-methyl	$C_{11}H_{16}$	148	8.627	2.49	89
6	3H-1,2,4-triazol-3-one, 4-amino-2,4-dihydro-2-methyl-5-phenyl	$C_9H_{10}N_4O$	190	14.690	0.74	75
7	Decanoic acid, methyl ester	$C_{11}H_{22}O_2$	186	18.251	0.88	87
8	2-Hexadecen-1-ol, 3,7,11,15-tetramethyl-, [R]	$C_{20}H_{40}O$	296	20.056	10.61	97
9	Bis(trimethylsilyl) ether of 1,4-anhydro-3-deoxypentitol	$C_{11}H_{26}O_3Si_2$	262	25.511	0.84	59
10	D-erythro-pentopyranose, 2-deoxy-1,3,4-tris-o-(trimethylsilyl)	$C_{14}H_{34}O_4Si3$	350	26.933	1.23	57
11	5-Hydroxymethyl-2,2,5-trimethyl-1,3-dioxane,	$C_{11}H_{24}O_3Si$	232	26.332	0.76	56
12	Cis-4-Trimethylsilyloxy-cyclohexyl(trimethylsilyl)carboxy	$C_{13}H_{28}O_3Si_2$	288	28.086	0.75	50
13	(1-butoxybutoxy)trimethylsilane	$C_{11}H_{26}O_2Si$	218	13.590	0.90	74
14	Phytol, acetate	$C_{22}H_{42}O_2$	338	20.562	5.95	76
15	D-Erythro-Pentofuranose, 2-deoxy-1,3,5-tris-O-(trimethylsilyl)	$C_{14}H_{34}O_4Si3$	350	27.051	2.02	55

Proposed mechanism of CI

KBE protected MS against corrosion in a 0.5 M H_2SO_4 solution by the adsorption process. CI mechanism is based on molecules interactions of acceptor and donor electrons between KBE and unoccupied d- orbital's on the MS surface. In other words, KBE's hetero atoms interacted with the vacant d-orbital of the MS surface. At higher Ct, Its CI potential in AE, namely H_2SO_4, was stronger [54].

Conclusions

KBE showed excellent CI results against MS corrosion in a 0.5 M H_2SO_4 solution. Its IE(%) increased with higher Ct. The highest IE(%) of 98.41% was observed for the Ct of 1600 ppm. All electrochemical measurements showed an analogous trend of IE(%). KBE adsorption onto the MS surface obeyed Langmuir's isotherm. It was a monolayer adsorption, and its nature was spontaneous and comprehensive. Surface morphology study via SEM confirmed the MS surface improvement, due to KBE adsorption onto it. KBE corrosion protection of MS, at particularly low Ct, makes it an ideal material for creating self-healing coatings.

Authors' contributions

O. S. Yadav: planned the original research works; performed experiments and analysis; interpreted the results; wrote the manuscript. **S. Kumar and K. Yadav**: treated experimental data; validated results; prepared the draft. **R. Sharma and R. Kumar**: validated results; prepared the draft.

Acknowledgment

This research work was supported by Prof. Rabi Narayan Kar Shyamlal of College University of Delhi. All the authors also would like to thank DBT-Star Scheme College for financial support of the Department of Chemistry Shyamlal College and the University Science Instrumentation Centre (USIC), University of Delhi, India, and JNU, for research facilities.

Abbreviations

AE: acidic environment
AFM: atomic force microscopy
C_{dl}: double layer capacitance
CI: corrosion inhibitor
C_{inh}: inhibitor concentration
CPE: constant phase element
CR: corrosion rate
Ct: concentration
E_{corr}: corrosion potential
EIS: electrochemical impedance spectroscopy
GC-MS: gas chromatography/mass spectrometry
H_2SO_4: sulfuric acid

HER: hydrogen evolution reaction
i_{corr}: corrosion current density
IT: immersion time
KB: *Kala Bansa* (*Barleria Prionitis*)
KBE: *Kala Bansa*extract
LPR: linear polarization resistance
MF: molecular formula
MS: mild steel
MW: molecular weight
OCP: open circuit potential
PA: peak area
PDP: potentiodynamic polarization
ppm: parts per million
R^2: regression coefficient
R_{ct}: charge transfer resistance
SC: surface coverage
SEM: scanning electron microscopy
SI: similarity index
SR: scan rate
T: temperature
WL: weight loss

Symbols definition
β_a: anodic Tafel slope
β_c: cathodic Tafel slope
$\Delta G°_{ads}$: standard free energy for Gibbs
$\Delta H°_{ads}$: standard enthalpy
$\Delta S°_{ads}$: standard entropy
E_a: activation energy for Arrhenius equation

References

1. Koch G. Cost of corrosion: In Trends in Oil and Gas Corrosion Research and Technologies. Elsevier. 2017;2017:3-30. https://doi.org/10.1016/B978-0-08-101105-8.00001-2
2. Quraishi MA, Sardar R. Aromatic tri azoles as corrosion inhibitors for mild steel in acidic environments. Corrosion. 2002:58(9):748-755. https://doi.org/10.5006/1.3277657
3. Yadav M, Sharma U, Yadav PN. Isatin compounds as corrosion inhibitors for N 80 steel in 15% HCl. Egypt J Pet. 2013;(22)3:335-344.
4. Obot IB, Meroufel A, Onyeachu IB et al. Corrosion inhibitors for acid cleaning of desalination heat exchangers: Progress, challenges and future perspectives. J Mol Liq. 2019;296:111760. https://doi.org/10.1016/j.molliq.2019.111760

5. Hooshmand ZS, Sharifi M, Zaarei D et al. Application of eco-friendly products as corrosion inhibitors for metals in acid pickling processes–A review. J Environ Chem Eng. 2013;1(4):652-657. https://doi.org/10.1016/j.jece.2013.09.019
6. Naveen E, Ramnath BV, Elanchezhian C et al. Influence of organic corrosion inhibitors on pickling corrosion behaviour of sinter-forged C45 steel and 2% Cu alloyed C45 steel. J Alloy Compd. 2017;695:3299-3309. https://doi.org/10.1016/j.jallcom.2016.11.133
7. Shahmoradi AR, Ranjbarghanei M, Javidparvar AA et al. Theoretical and surface/electrochemical investigations of walnut fruit green husk extract as effective inhibitor for mild-steel corrosion in 1 M HCl electrolyte. J Mol Liq. 2202;338:116550. https://doi.org/10.1016/ j.molliq.2021;(338):116550
8. Shahini MH, Ramezanzadeh M, Ramezanzadeh B et al. The role of ethanolic extract of *Stachys byzantina's* leaves for effective decreasing the mild-steel (MS) degradation in the acidic solution; coupled theoretical/experimental assessments. Mol Liq. 2021;329:115571. https://doi.org/10.1016/j.molliq.2021
9. Shahini MH, Ramezanzadeh M, Bahlakeh G et al. Superior inhibition action of the Mish Gush (MG) leaves extract toward mild steel corrosion in HCl solution: Theoretical and electrochemical studies. J Mol Liq. 2021;332:115876. https://doi.org/10.1016/j.molliq.2021
10. Lashgari SM, Bahlakeh G, Ramezanzadeh B. Detailed theoretical DFT computation/molecular simulation and electrochemical explorations of *Thymus vulgaris* leave extract for effective mild-steel corrosion retardation in HCl solution. J Mol Liq. 2021;335:115897. https://doi.org/10.1016/ j.molliq.2021
11. Dehghani A, Bahlakeh G, Ramezanzadeh B et al. *Aloysia citrodora* leaves extract corrosion retardation effect on mild-steel in acidic solution: Molecular/atomic scales and electrochemical explorations. J Mol Liq. 2020;310:113221. https://doi.org/10.1016/j.molliq.2020
12. Bhardwaj N, Sharma P, Guo L et al. Molecular dynamic simulation, quantum chemical calculation and electrochemical be haviour of *Punica granatum* peel extract as eco friendly corrosion inhibitor for stainless steel (SS-410) in acidic medium. J Mol Liq. 2022;346:118237. https://doi.org/10.1016/j.molliq.2021.118237
13. Aourabi S, Driouch M, Sfaira M, Guo L et al. Phenolic fraction of *Ammi visnaga* extract as environmentally friendly antioxidant and corrosion inhibitor for mild steel in acidic medium. J Mol Liq. 2021;323:114950. https://doi.org/10.1016/j.molliq.2020.114950
14. Mushira BA, Arifa FB, Riaz AK. Evaluation of inhibitive performance of *Allamanda cathartica* leaves extract as a green corrosion inhibitor on mild steel in acid medium. Mat Tod: Proceed. 2021;47:2036-2047. https://doi.org/10.1016/j.matpr.2021.04.372

15. Anggraini EL, Stiadi Y, Zulaiha S et al. Stainless 37 Steel Corrosion Inhibition in a Hydrochloric Acid Solution with Senggani (*Melastoma Candidum D. Don*) Leaf Extract. Port Electrochim Acta. 2023;41:199-210. https://doi.org/10.4152/pea.2023410302
16. Khadom AA, Ahmed NA, Mustafa M et al. Combined influence of iodide ions and *Xanthium Strumarium* leaves extract as eco-friendly corrosion inhibitor for low-carbon steel in hydrochloric acid. Curr Res Green Sustain Chem. 2022;5:100278. https://doi.org/10.1016/j.crgsc.2022.100278
17. Banerjee S, Banerjee S, Gaurab K Jha et al. *Barleria Prionitis L.*: An Illustrative Traditional, Phytochemical and Pharmacological Review. Nat Prod J. 2021;11(3):258-274. https://doi.org/10.2174/2210315510666200131114525
18. Kumar R, Yadav OS, Singh G. Electrochemical and surface characterization of a new eco-friendly corrosion inhibitor for mild steel in acidic media: a cumulative study. J Mol Liq. 2017:237:413-427. https://doi.org/10.1016/j.molliq.2017.04.103
19. Kumar R, Chopra R, Singh G. Electrochemical, morphological and theoretical in-sights of a new environmentally benign organic inhibitor for mild steel corrosion in acidic media. J Mol Liq. 2017:241:9-19. https://doi.org/10.1016/j.molliq.2017.05.130
20. Kumar R, Kim H, Singh G. Experimental and theoretical investigations of a newly synthesized azomethine compound as inhibitor for mild steel corrosion in aggressive media: a comprehensive study. J Mol Liq. 2018;259:199-208. https://doi.org/10.1016/j.molliq.2018.02.123
21. Bhadani A, Misono T, Singh S et al. Structural diversity, physicochemical properties and application of imidazolium surfactants: Recent advances. Adv Coll Interf Sci. 2016;231:36-58. https://doi.org/10.1016/j.cis.2016.03.005
22. Odewunmi NA, Umoren SA, Gasem ZM. Utilization of watermelon rind extract as a green corrosion inhibitor for mild steel in acidic media. J Ind Eng Chem. 2015;21:239-247. https://doi.org/10.1016/j.jiec.2014.02.030
23. Baggaa Kaur M, Gadib R, Yadav OS et al. Investigation of phytochemical components and corrosion inhibition property of *Ficus racem*osa stem extract on mild steel in H_2SO_4 medium. J Environ Chem Eng. 2016;4:4699-4707. https://doi.org/10.1016/j.jece.2016.10.022
24. Singh G, Adeyemi OO. Galvanostatic polarization and resistance studies of acid corrosion of commercial copper in the presence of some heterocyclic compounds. J Surf Sci Technol. 1987;3:121-132.
25. Abdallah M, Eltass M, Hegazy M et al. Adsorption and inhibition effect of novel cationic surfactant for pipelines carbon steel in acidic solution. Prot Met Phys Chem. 2016;(52)4:721-730. https://doi.org/10.1134/S207020511604002X
26. Deslouis C, Tribollet B, Mengoli G et al.Electrochemical behaviour of copper in neutral aerated chloride solution. I. Steady-state investigation. J Appl Electrochem. 1988:18:374-383. https://doi.org/10.1007/BF01093751

27. Oguzie EE, Lia Y, Wang FH. Effect of 2-amino-3-mercaptopropanoic acid (cysteine) on the corrosion behavior of low carbon steel in sulphuric acid. Electrochim Acta. 2007;53:909-914. https://doi.org/10.1016/j.electacta.2007.07.076
28. Shaban SM, Elbhrawy M, Fouda A et al. Corrosion inhibition and surface examination of carbon steel 1018 via N-(2-(2- hydroxyethoxy) ethyl)-N, N-dimethyloctan-1-aminium bromide in 1.0 M HCl. J Mol Struct. 2021;1227:129713. https://doi.org/10.1016/j.molstruc.2020.129713
29. Javadian S, Yousefi A, Neshati J. Synergistic effect of mixed cationic and anionic surfactants on the corrosion inhibitor behavior of MS in 3.5% NaCl. Appl Surf Sci. 2013;285:674-681. https://doi.org/10.1016/j.apsusc.2013.08.109
30. Mahdavian M, Tehrani-Bagha AR, Alibakhshia E et al. Corrosion of MS in hydrochloric acid solution in the presence of two cationic gemini surfactants with and without hydroxyl substituted spacers. Corros Sci. 2018;137:62-75. https://doi.org/10.1016/j.corsci.2018.03.034
31. Khodyrev Y P, Batyeva ES, Badeeva EK et al. The inhibition action of ammonium salts of O,O ′ dialkyl dithiophosphoric acid on carbon dioxide corrosion of mild steel. Corros Sci. 2011;53:976-983. https://doi.org/10.1016/j.corsci.2010.11.030
32. Oguzie EE, Li Y, Wang FH. Corrosion inhibition and adsorption behavior of methionine on mild steel in sulfuric acid and synergistic effect of iodide ion. J Coll Interf Sci. 2007;310:90-98. https://doi.org/10.1016/j.jcis.2007.01.038
33. Okafor PC, Zheng YG. Synergistic inhibition behavior of methylbenzyl quaternary imidazoline derivative and iodide ions on mild steel in H_2SO_4 solutions. Corros Sci. 2009;51:850-859. https://doi.org/10.1016/j.corsci.2009.01.027
34. Chopra R, Kansal K, Kumar R et al. Electrochemical, morphological and anti–corrosive characteristics of pyrazine derivatives for mild steel corrosion in aggressive medium: a comparative study. J Fail Analyt Prev. 2018;18:1411-1428. https://doi.org/10.1007/s11668-018-0527-0
35. Flory PJ. Thermodynamics of high polymer solutions. J Chem Phys. 1942;10:51-61. https://doi.org/10.1063/1.1723621
36. Okafor PC, Liu CB, Liu X et al. Corrosion inhibition and adsorption behavior of imidazoline salt on N80 carbon steel in CO_2-saturated solutions and its synergism with thiourea. J Solid State Electrochem. 2010;14:1367-1376. https://doi.org/10.1007/s10008-009-0963-6
37. Bentiss F, Jama C, Mernari B et al. Corrosion control of mild steel using 3,5-bis(4-methoxyphenyl)-4-amino-1,2,4-triazole in normal hydrochloric acid medium. Corros Sci. 2009;51:1628-1635. https://doi.org/10.1016/j.corsci.2009.04.009
38. Bellman C. Polymer Surfaces and Interfaces. M. Stamm, Springer, Berlin, 2008.

39. Zhu H, Li X, Lu X et al. Efficiency of Gemini surfactant containing semi-rigid spacer as microbial corrosion inhibitor for carbon steel in simulated seawater. Bio Electrochem. 2021;140:107809. https://doi.org/10.1016/j.bioelechem.2021.107809
40. Tawfik SM. Ionic liquids based gemini cationic surfactants as corrosion inhibitors for carbon steel in hydrochloric acid solution. J Mol Liq. 2016;216:624-635. https://doi.org/10.1016/j.molliq.2016.01.066
41. Mishrif MR, El-Din MN, Khamis E. Utilization of ethoxylated pentamine oleamide as new Gemini surfactants for corrosion inhibition effectiveness in 1 M HCl solution. Egypt J Pet. 2018:(27)4:1357-1370.
42. Martinez S, Stern I. Thermodynamic characterization of metal dissolution and inhibitor adsorption processes in the low carbon steel/mimosa tannin/sulfuric acid system. Appl Surf Sci. 2002;199:83-89. https://doi.org/10.1016/S0169-4332(02)00546-9
43. Mourya P, Banerjee S, Rastogi RB et al. Inhibition of Mild Steel Corrosion in Hydrochloric and Sulfuric Acid Media Using a Thio semicarbazone Derivative. Ind Eng Chem Res. 2013;52(36):12733-12747. https://doi.org/10.1021/ie4012497
44. Yadav M, Behera D, Kumar S et al. Experimental and quantum chemical studies on corrosion inhibition performance of thiazolidinedione derivatives for mild steel in hydrochloric acid solution. Chem Eng Commun. 2014;(202)3:303-315. https://doi.org/10.1080/00986445.2013.841148
45. Eddy NO, Ameh P, Gimba CE et al. GCMS studies on *Anogessus leocarpus* (Al) gum and their corrosion inhibition potential for mild steel in 0.1 M HCl. Int J Electrochem Sci. 2011;6(11):5815-5829. https:// doi.org/10.1016/S1452-3981(23)18447-1
46. Singh G, Arora SK, Mathur S P. Eco-friendly corrosion inhibition of mild steel in hydrochloric acid using *Leptadenia pyrotechnica* as a Green inhibitor. Res J Chem Sci. 2015:5(8):28-34. https://www.isca.in/rjcs/Archives/v5/i8/6.ISCA-RJCS-2015-108.pdf
47. Shyamala M, Kasthuri PK. The inhibitory action of the extracts of *Adathodavasica*, *Eclipta alba*, and *Centella asiatica* on the corrosion of mild steel in hydrochloric acid medium: a comparative study. Int J Corros. 2011:2012:ID 852827:1-13. https://doi.org/10.1155/2012/852827
48. Rocha JC, Cunha JA, Gomes P et al. Aqueous extracts of mango and orange peel as green inhibitors for carbon steel in hydrochloric acid solution. Mater Res. 2014;17(6):1581-1587. https://doi.org/10.1590/1516-1439.285014
49. Eddy NO, Ameh P, Gimba CE et al. Chemical information from GCMS of *Ficus platyphylla* Gum and its corrosion inhibition potential for mild steel in 0.1 M HCl. Int J Electrochem Sci. 2012;7:5677-5691. https://doi.org/10.1016/s1452-3981(23)19651-9

50. Ibrahim T, Gomes E, Obot IB et al. Corrosion inhibition of mild steel by *Calotropis procera* leaves extract in a CO_2 saturated sodium chloride solution. J Adhes Sci Technol. 2016;30(23):2523-2543. https://doi.org/10.1080/01694243.2016.1185229.
51. Raja PB, Sethuraman MG. Inhibition of corrosion of mild steel in sulphuric acid medium by *Calotropis procera*. Pigm Resin Technol. 2009;38:33-37. https://doi.org/10.1108/03699420910923553
52. Torres AR, Cisneros MGV, Rodríguez JGG. *Medicago sativa* as a green corrosion inhibitor for 1018 carbon steel in 0.5 M H_2SO_4 solution. Green Chem Lett Rev. 2016;9:143-155. https://doi.org/10.1080/17518253.2016.1195017
53. Eddy NO. Ethanol extract of *Phyllanthus amarus* as a green inhibitor for the corrosion of mild steel in H_2SO_4. Port Electrochim Acta. 2009:27(5):579-589. https://doi.org/10.4152/pea.200905579
54. Bhardwaj N, Sharma P, Guo L et al. Molecular dynamic simulation and quantum chemical calculation of phytochemicals present in *Beta vulgaris* and electrochemical behavior of *Beta vulgaris* peel extract as green corrosion inhibitor for stainless steel (SS-410) in acidic medium. Colloids Surf. 2022;632:127707. https://doi.org/10.1016/j.colsurfa.2021.127707